A. Colagrossi, M. Lavagna
Fully Magnetic Attitude Control Subsystem for Picosat Platforms
Advances in Space Research, Vol. 62, N. 12, 2018, p. 3383-3397
doi:10.1016/j.asr.2017.10.022

Fully Magnetic Attitude Control Subsystem for Picosat Platforms

Andrea Colagrossi*, Michèle Lavagna

Aerospace Science and Technology Department, Politecnico di Milano, Via La Masa, 34, 20156, Milan, Italy

Abstract

In this paper, the design of a fully magnetic attitude control subsystem for a picosat platform is discussed. The developed control law is based on a simple and reliable architecture, which can be easily implemented on small spacecrafts for de-tumbling and three-axis stabilization purposes. The subsystem design follows a practical engineering approach, exploiting global optimization methods, which lead to an integral actuation compliant with typical pointing accuracy requirements for picosat missions. Performance of the proposed attitude control subsystem is demonstrated by numerical simulations.

Keywords: Active Attitude Control, Magnetorquer, Picosat, Integral Actuation, Global Optimization Methods

1. Introduction

Small spacecraft missions are experiencing an increasing interest from the space community, since their capability to reduce the cost of space access while performing operations only possible in the past with larger and heavier satellites. In particular, miniaturization of spacecraft components nowadays allows to integrate fully operational spacecrafts weighing less than a kilogram, which are usually referred to as *picosatellites* or *picosats*.

*Corresponding author
Email addresses: andrea.colagrossi@polimi.it (Andrea Colagrossi), michelle.lavagna@polimi.it (Michèle Lavagna)

These small space systems obviously require to be de-tumbled immediately after the release from the orbital deployer, and to be often stabilized or controlled in attitude. However, their low inertia compared to the high density of electronics that strongly interacts with the Earth's magnetic field, determines their chaotic attitude motion and makes difficult to exploit gravity gradient or spinning stabilization techniques (Inamori et al., 2011). For these reasons, an active attitude control subsystem is frequently needed to de-tumble, stabilize and control small spacecrafts. Despite many possible approaches to the control of attitude dynamics have been developed through the years, a particularly effective and reliable one is constituted using electromagnetic actuators. This control strategy is especially suitable for picosatellites, since they are usually operated in low Earth orbits (LEOs), where a strong geomagnetic field is present. Moreover, it helps to save overall power, weight, cost and complexity compared to other techniques based on thrusters or moving parts (e.g. reaction wheels). Furthermore, the simplicity of magnetic control allows to reduce the risk of failure and, therefore, the entire space system is more reliable. Certainly, the magnetic control can be either active or passive, but the latter does not allow to have many degrees of freedom for attitude control and spacecraft maneuvers. For all these reasons, a fully magnetic active attitude control subsystem for picosats is presented in this paper.

Electromagnetic actuators constitute the distinctive element of any magnetic attitude control subsystem. They are essentially electromagnetic coils generating an asymmetric time-variable magnetic field. That field is controlled by varying the input currents of the electromagnets, according to the implemented closed-loop feedback control law. The coil can be wound around a ferromagnetic core, usually shaped as a rod and denoted as *magnetic torque rod*, or it can be a simple thin coil that can be also embedded in the electronic board (e.g. Printed Circuit Board - PCB). In this last situation, the actuator is typically called *air-core coil*, but in general all these electromagnetic actuators are indicated as *magnetorquers*.

The spacecraft attitude is controlled thanks to the interaction between the magnetic dipole moment, $\mathbf{d}$, generated by a set of three orthogonal magnetorquers and the Earth's magnetic field, $\mathbf{b}$. The control torque is therefore simply obtained as $\mathbf{t}_{mag} = \mathbf{d} \times \mathbf{b}$ (Wertz, 1978). From this equation, it is evident the main drawback of the magnetic attitude control technique: the control torque is always constrained to lie in the plane orthogonal to the local geomagnetic field vector. Therefore, a spacecraft controlled with electromagnetic actuators would be always a locally under-actuated system

(Sidi, 1997; Markley and Crassidis, 2014). In spite of this, if the spacecraft operational orbit is inclined enough with respect to the geomagnetic equator, the Earth's magnetic field vector has a periodic motion with respect to the orbital reference frame and, consequently, it is possible to apply torques, in average over one orbital period, in any direction and, thus, the spacecraft can be stabilized (Bhat and Dham, 2003).

The application of magnetic attitude control has been deeply investigated since the early stages of astronautics (White et al., 1961), both for attitude control and for reaction wheels' momentum dumping. Nevertheless, until the last decade of the 20^{th} century, only approximate solutions of the control with magnetorquers were existing in literature (Stickler and Alfriend, 1976; Musser and Ebert, 1989). Just in the first decade of the new millennium, with the explosion of small satellites missions, the interest of the international space community was directed toward magnetic actuators for spacecraft attitude control (Wiśniewski and Blanke, 1999; Lovera et al., 2002; Lovera and Astolfi, 2004; Silani and Lovera, 2005). Both linear and non-linear attitude control problems have been investigated, considering LQ control techniques, Lyapunov methods, model predictive approaches and many theorems for attitude stability.

As a result, if closed-loop dynamics is sufficiently slow, conventional proportional derivative control law can be applied. However, if large rotations or high angular rates (e.g. initial satellite de-tumbling), high nonlinearities are involved and nonlinear control techniques are needed (Cubas et al., 2015). In particular, it should be noted that one of the most used nonlinear strategies is the well-known B-dot control law (Stickler, 1972; Stickler and Alfriend, 1976), which is characterized by its simplicity and is very effective to dump the spacecraft's angular velocity (Flatley et al., 1997). In fact, with this nonlinear control law, the commanded magnetorquers dipole is proportional to the derivative of the geomagnetic field, and this results in a dissipative effect that decreases the kinetic energy of the spacecraft. But, using this control law, the angular velocity of the satellite cannot be stabilized at a particular chosen value, and the B-dot strategy lacks of control regarding the final attitude of the satellite. In recent years, some studies have been conducted and improved versions of the B-dot control law have been presented (Avanzini and Giulietti, 2012).

In this paper, a fully magnetic attitude control subsystem, which makes use of the conventional proportional derivative (PD) control together with a modified B-dot control, is presented. The method has been developed to

be implemented on picosatellites, having in mind the idea to maintain the attitude control subsystem as simple and reliable as possible. Obviously, the method increases the complexity of the classical B-dot control, because the on-board computer has to store additional information (e.g. the Earth's magnetic field model) and has to estimate the position and the orientation of the spacecraft, allowing an attitude control logic capable to de-tumble, stabilize and control a picosatellite in LEO.

The subsystem design has followed a practical engineering approach, which had to be robust and easily applicable to different small satellite missions. The method has been developed directly exploiting a high-fidelity dynamical model, including the perturbations relevant for a selected operative environment. This approach obviously provided less general results, but considering the method which has been used to implement it, the outcomes can be easily applied to any other similar scenario. Furthermore, in this way, the attitude subsystem is immediately available for testing and integration on real systems.

Global optimization methods have been used to tune the subsystem parameters on a particular mission scheme. The paper accurately describes the tuning process, which is part of the presented method, to obtain the actuation logic of the magnetorquers that is able to guarantee integral performances over one orbital period, compliant with typical requirements for picosat missions.

The design of the attitude control subsystem (ACS) has been carried out in parallel with the design of the attitude determination subsystem (ADS), in order to have a global overview on the mutual requirements and constraints between the two subsystems. In this paper, the focus is on the ACS and the ADS is just briefly introduced to have an idea on the quantities that are used to control the attitude of the picosatellite.

2. Dynamical Model

The dynamical model that is used to develop the attitude control subsystem is based on Euler's equation for rigid spacecrafts, expressed in the body reference frame, B. The attitude of the spacecraft is referenced to an Earth-centered inertial (ECI) frame, I, through a direction cosine matrix, $\mathbf{A}$. Moreover, since small satellites often carry out Earth missions, the attitude is also referenced to a local-vertical-local-horizontal (LVLH) frame, L_{VH}, through a rotation matrix, $\mathbf{P}$.

As shown in fig. 1, the inertial reference frame has the origin, O, coinciding with the center of the Earth, $\hat{\mathbf{x}}$ pointing toward Vernal equinox, $\hat{\mathbf{z}}$ parallel

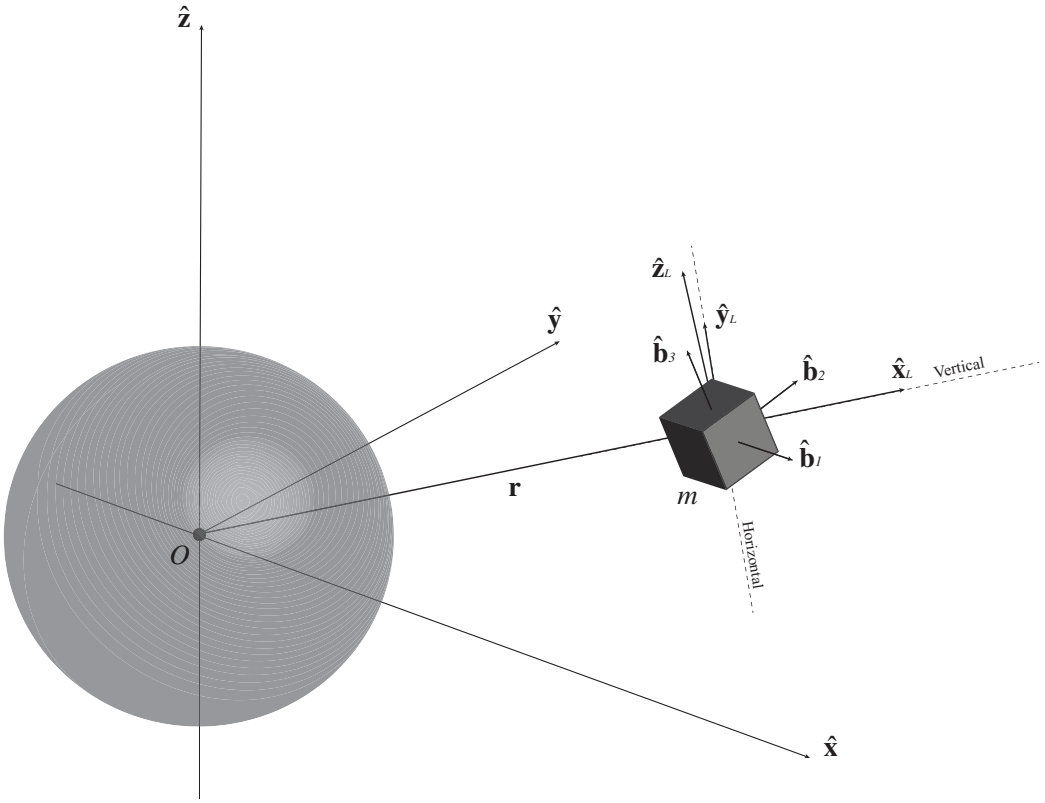

Figure 1: Earth-centered inertial (ECI), local-vertical-local-horizontal (LVLH) and body-fixed reference frames.

to the Earth's rotational axis pointing toward north and $\hat{\mathbf{y}}$ completing the right-hand Cartesian frame. The center of mass of the spacecraft, O_B, can be univocally positioned in I by the radius vector, $\mathbf{r}$, which is also defining the origin of the two other reference frames. In fact, the LVLH frame is centered in O_B, it has the first axis, $\hat{\mathbf{x}}_L$ aligned with the vector $\mathbf{r}$, the second axis, $\hat{\mathbf{z}}_L$, along the orbit normal and the third axis, $\hat{\mathbf{y}}_L$, completing the right-hand triad in the horizontal direction. The body-fixed frame B is centered at the center of mass of the spacecraft, O_B, and it is aligned with the body principal inertia directions, $\hat{\mathbf{b}}_1$, $\hat{\mathbf{b}}_2$ and $\hat{\mathbf{b}}_3$.

The position vector is initialized considering the starting position on the selected operational orbit. Then, it is propagated in time integrating the perturbed equation of two-body motion. This allow to know the position of the spacecraft with respect to the Earth at any instant of time. The

perturbations are directly inserted in the equations of motion and, from the resulting acceleration on the spacecraft, the orbital path is found: Cowell's method (Bate et al., 1971). Further details on the perturbations used in the simulations will be discussed later in the paper. The position of the spacecraft is needed to gather information on the expected geomagnetic field from the models and to obtain other kinematic data to be used in the attitude determination process.

As already said, the attitude dynamics is propagated in time using the Euler's equation of rigid body motion:

$$\mathbf{I}\dot{\boldsymbol{\omega}} = -\boldsymbol{\omega} \times \mathbf{I}\boldsymbol{\omega} + \mathbf{t}_{mag} + \mathbf{t}_d, \tag{1}$$

where $\boldsymbol{\omega} = [\omega_1, \omega_2, \omega_3]^{\mathrm{T}}$ is the vector of spacecraft angular velocity, expressed in body frame, $\mathbf{I}$ is the inertia matrix, $\mathbf{t}_{mag}$ is the vector of magnetic control torque and $\mathbf{t}_d$ is the vector of external disturbance torques.

The disturbance phenomena that are considered in the simulations affects both the orbital and the attitude dynamics, in a way that the fidelity of the simulations is high enough for ACS design purposes. The orbital perturbations used in the model include the irregularities in the gravitational potential due to non-spherical distribution of Earth's mass, the presence of the Moon and the Sun as third and fourth bodies, the effect of the solar radiation pressure (SRP) and the atmospheric drag. For what concern the disturbance related with the rotational dynamics, $\mathbf{t}_d$ is composed by the gravity gradient torque exerted by the Earth, the Moon and the Sun on the small spacecraft, the geomagnetic field interaction with the spurious dipole of the satellite, the SRP torque and the atmospheric drag torque. The Earth gravitational model is the NGA/EGM2008, used with harmonics up to the fourth degree and order. The third and fourth body contributions are computed considering the ephemeris positions of the Moon and the Sun contained in the SPICE Toolkit by NASA / JPL. The force that is generated by the solar radiation pressure interaction is computed for each face of the picosat, considering its real shape. Then, the global force can be found summing all over the single contributions, which are evaluated using the expression for the radiation pressure on a flat surface. The torque generated by the SRP is easily obtained knowing the offset of the faces with respect to the center of mass O_B. The SRP effect is evaluated exploiting the ephemeris position of the Sun. Similarly to the SRP, the aerodynamic disturbance is computed for any face of the spacecraft. In fact, knowing the orbital velocity of the spacecraft and its angular velocity,

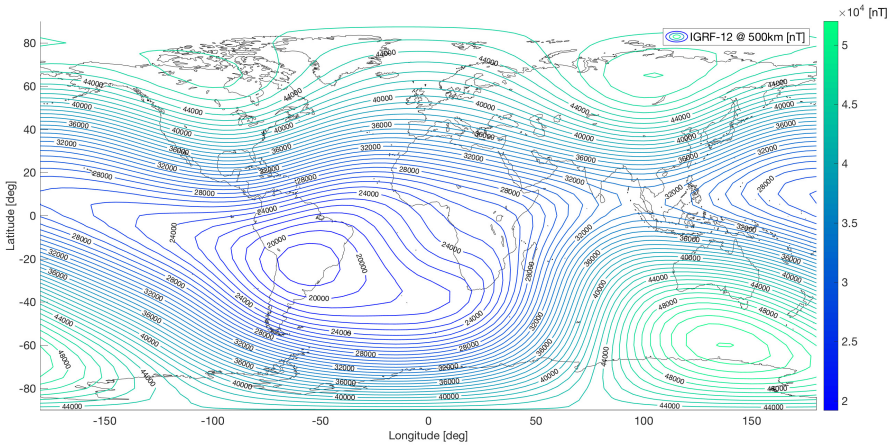

Figure 2: Earth's magnetic field model (IGRF-12) at 500 km of altitude.

the relative velocity of the faces of the satellite with respect to the airflow can be obtained. Then, the atmospheric drag force and torque are computed summing the contribution of each single planar face. The Jacchia Reference Atmosphere is used as atmospheric model. The Earth's magnetic field is obtained from the 12$^{\text{th}}$ edition of the International Geomagnetic Reference Field (IGRF-12). The series expansion is computed with all the harmonics available in the model, and the local value of the geomagnetic field is evaluated knowing the position of the spacecraft. Figure 2 shows the Earth's magnetic field model at 500 km of altitude. The internal dipole of the spacecraft is represented according to guidelines described in literature (Schalkowsky and Harris, 1969). Notwithstanding, considering the importance of this quantity, the performances of the ACS presented in this paper have been analyzed considering different internal dipole characteristics, as will be explained in the following. The perturbations have been modelled with the purpose to have the highest possible accuracy, and refined models of the environment and of the spacecraft have been used. With this method, the design parameters of the ACS were immediately available for the relevant operative environment. However, it is important to note that the simulations are not free from modeling errors, and higher order perturbations may lead to losses in the accuracy of the results. For this reason, sensitivity analyses have to be carried out during the test phase in order to check that the system meets the design requirements in any case.

The attitude of the spacecraft has been parametrized using the well-known Euler parameters, or quaternions, which lead to the following representation for the attitude kinematics:

$$\dot{\mathbf{q}} = \frac{1}{2}\mathbf{W}(\boldsymbol{\omega})\mathbf{q}, \tag{2}$$

where $\mathbf{q} = [q_1, q_2, q_3, q_4]^{\mathrm{T}}$ is the unit norm four components vector of Euler parameters and the matrix of angular velocity components, $\mathbf{W}(\boldsymbol{\omega})$ is expressed as:

$$\mathbf{W}(\boldsymbol{\omega}) = \begin{bmatrix} 0 & \omega_3 & -\omega_2 & \omega_1 \\ -\omega_3 & 0 & \omega_1 & \omega_2 \\ \omega_2 & -\omega_1 & 0 & \omega_3 \\ -\omega_1 & -\omega_2 & -\omega_3 & 0 \end{bmatrix}. \tag{3}$$

From the Euler parameters, the direction cosine matrix $\mathbf{A}$ can be obtained immediately. As well as the rotation matrix $\mathbf{P}$, which ca be easily computed from $\mathbf{A}$ and the position of the spacecraft along the operational orbit, expressed in terms of Keplerian parameters. Remember that $\mathbf{A}$ and $\mathbf{P}$ relate the body-fixed frame to the inertial frame and to the LVLH frame, respectively.

3. Attitude Control Subsystem

A fully magnetic attitude control system is actuated by a set of three magnetorquers, aligned with the spacecraft principal axes, which generate torques according to:

$$\mathbf{t}_{mag} = \mathbf{d} \times \mathbf{b} = \mathbf{B}(\mathbf{b})\mathbf{d}, \tag{4}$$

where $\mathbf{d}$ is magnetic dipole vector generated by the set of magnetorquers, $\mathbf{b}$ is the vector with components, b_1, b_2 and b_3, of the local geomagnetic field expressed in the body-fixed reference frame and the matrix $\mathbf{B}(\mathbf{b})$ is defined as:

$$\mathbf{B}(\mathbf{b}) = \begin{bmatrix} 0 & b_3 & -b_2 \\ -b_3 & 0 & b_1 \\ b_2 & -b_1 & 0 \end{bmatrix}. \tag{5}$$

The dipole generated by the magnetorquers is the control variable that the attitude control logic has to evaluate at any instant of time in order to correctly control the picosatellite. The dipole $\mathbf{d}$ is a vector in body reference frame and, in general, it has components along any principal inertia direction: $\mathbf{d} = [d_1, d_2, d_3]^{\mathrm{T}}$. Each magnetorquer produces a dipole moment in

a direction perpendicular to the plane of the coil and, since the three magnetic actuators are aligned with the principal inertia axes of the spacecraft, each electromagnetic coil generates a single component of the requested magnetic dipole moment. The magnitude of the dipole components can be obtained knowing the characteristics of each magnetorquer, in fact:

$$d_i = k_i \, A_i \, I_i = k_i \, A_i \, \frac{V_i}{R_i}, \quad \text{with} \quad i = 1, 2, 3, \tag{6}$$

where A_i is the area of the $i-$th coil, I_i is the current intensity sent to the magnetorquer and k_i is a coefficient dependent from the number of windings of the coil, the magnetic permeability of the core and other parameters related with shape and construction of the magnetorquer. Since the coil is often connected to a pulse-width modulation (PWM) voltage regulator, eq. (6) is more conveniently expressed in terms of coil voltage, V_i, and coil resistance, R_i. The latter is a constant parameter for a given electromagnetic actuator, while the former is the actual control variable to be computed from the attitude control logic for the PWM voltage regulator to correctly command the magnetorquers. In fact, once the required dipole is known the voltage for the magnetorquers, V_1, V_2 and V_3 are:

$$V_i = \frac{R_i}{k_i \, A_i} d_i, \quad \text{with} \quad i = 1, 2, 3. \tag{7}$$

However, this is the last step of the picosatellite attitude control logic, which is working in the loop immediately after the attitude determination process. The developed attitude determination system for picosatellites, which will be presented in a different publication, is based on simple sensors (e.g. Sun sensors, magnetometers, Inertial Measurements Units - IMU) and it makes available for the ACS the estimated orbital position, $\tilde{\mathbf{r}}$, the estimated angular velocity in B, $\tilde{\boldsymbol{\omega}}$, and the estimated rotation matrices, $\tilde{\mathbf{A}}$ and $\tilde{\mathbf{P}}$. These quantities are used in the first part of the guidance section to evaluate the errors with respect to the imposed target dynamics.

The complete target attitude is composed by two orthogonal directions to be aligned with two orthogonal body-fixed axes and a desired spinning axis and rate. With a proper choice of these three conditions it possible to actuate a three-axis control strategy, obviously, the target must be formulated in a way that the different conditions are physically possible (e.g. spinning rate compatible with the target directions motion). Moreover, if one or two target

conditions are not needed, they can be removed from the ACS logic that is able to control the spacecraft also along a less constrained target dynamics (e.g. spinning axis and rate without imposed target directions).

In general, the target is expressed in body-fixed frame as:

$$\mathbf{v}_{T_1}^B = \alpha_1\hat{\mathbf{b}}_1 + \alpha_2\hat{\mathbf{b}}_2 + \alpha_3\hat{\mathbf{b}}_3 \tag{8}$$

$$\mathbf{v}_{T_2}^B = \beta_1\hat{\mathbf{b}}_1 + \beta_2\hat{\mathbf{b}}_2 + \beta_3\hat{\mathbf{b}}_3 \tag{9}$$

$$\boldsymbol{\omega}_T^B = \omega_T(\gamma_1\hat{\mathbf{b}}_1 + \gamma_2\hat{\mathbf{b}}_2 + \gamma_3\hat{\mathbf{b}}_3), \tag{10}$$

where the coefficients α_i, β_i and γ_i with $i = 1, 2, 3$ allow to have a target direction which is a linear combination of the body frame axes. The quantity ω_T is the desired angular rate.

The target is associated with a particular physical direction which is usually defined and available from the models in the inertial reference frame (e.g. Sun direction, Earth center direction, orbital velocity direction). The output of the attitude determination is therefore used to evaluate the actual target directions and angular velocity in body frame as:

$$\breve{\mathbf{v}}_{T_1}^B = \tilde{\mathbf{A}}\mathbf{v}_1^I = \tilde{\mathbf{P}}\mathbf{v}_1^{LVH} \tag{11}$$

$$\breve{\mathbf{v}}_{T_2}^B = \tilde{\mathbf{A}}\mathbf{v}_2^I = \tilde{\mathbf{P}}\mathbf{v}_2^{LVH} \tag{12}$$

$$\breve{\boldsymbol{\omega}}_T^B = \tilde{\boldsymbol{\omega}}, \tag{13}$$

where $\mathbf{v}_1^I$, $\mathbf{v}_2^I$ and $\mathbf{v}_1^{LVH}$ and $\mathbf{v}_2^{LVH}$ are the target physical directions respectively in inertial and LVLH frame, $\tilde{\mathbf{A}}$ and $\tilde{\mathbf{P}}$ are the estimated rotation matrices and $\tilde{\boldsymbol{\omega}}$ is the estimated satellite's angular velocity in B.

The attitude control subsystem goal consists in having the actual target directions and angular velocity aligned with the desired target vectors in principal inertia axes. Therefore, the guidance law is defined to maneuver the spacecraft to obtain:

$$\breve{\mathbf{v}}_{T_1}^B \longrightarrow \mathbf{v}_{T_1}^B \tag{14}$$

$$\breve{\mathbf{v}}_{T_2}^B \longrightarrow \mathbf{v}_{T_2}^B \tag{15}$$

$$\breve{\boldsymbol{\omega}}_T^B \longrightarrow \boldsymbol{\omega}_T^B. \tag{16}$$

The previous expressions mean that the actual physical quantities, $\breve{\mathbf{v}}_{T_1}^B$, $\breve{\mathbf{v}}_{T_2}^B$, $\breve{\boldsymbol{\omega}}_T^B$ have to be progressively aligned in body reference frame such that their vector components in B are equal to the right-hand side of eqs. (8) to (10).

Therefore, since $\breve{\mathbf{v}}_{T_1}^B$, $\breve{\mathbf{v}}_{T_2}^B$, $\breve{\boldsymbol{\omega}}_T^B$ and $\mathbf{v}_{T_1}^B$, $\mathbf{v}_{T_2}^B$, $\boldsymbol{\omega}_T^B$ are in general not aligned, it is possible to define some error quantities that are used to define the guidance law. The error in target directions is defined as an error axis and angle in a way that, if the spacecraft is rotated around the error axis for an angle equal to the error angle, the actual target direction is aligned with the desired one. Basically, the algorithm evaluates the axis-angle representation of the rotation between the actual and the desired target direction, and then converts it in an error rotation matrix exploiting the Rodrigues' rotation formula.

The algorithm to compute the error in $i-$th target direction begins computing the error axis, $\hat{\mathbf{e}}_i$, and angle, θ_{e_i}:

$$\hat{\mathbf{e}}_1 = \frac{\breve{\mathbf{v}}_{T_1}^B \times \mathbf{v}_{T_1}^B}{\left\| \breve{\mathbf{v}}_{T_1}^B \times \mathbf{v}_{T_1}^B \right\|}, \qquad \theta_{e_1} = \arccos\left(\frac{\breve{\mathbf{v}}_{T_1}^B}{\left\| \breve{\mathbf{v}}_{T_1}^B \right\|} \cdot \frac{\mathbf{v}_{T_1}^B}{\left\| \mathbf{v}_{T_1}^B \right\|} \right) \tag{17}$$

$$\hat{\mathbf{e}}_2 = \frac{\breve{\mathbf{v}}_{T_2}^B \times \mathbf{v}_{T_2}^B}{\left\| \breve{\mathbf{v}}_{T_2}^B \times \mathbf{v}_{T_2}^B \right\|}, \qquad \theta_{e_2} = \arccos\left(\frac{\breve{\mathbf{v}}_{T_2}^B}{\left\| \breve{\mathbf{v}}_{T_2}^B \right\|} \cdot \frac{\mathbf{v}_{T_2}^B}{\left\| \mathbf{v}_{T_2}^B \right\|} \right). \tag{18}$$

Then, the error matrix, $\mathbf{E}_i$, is simply obtained as:

$$\mathbf{E}_1 = \mathbf{I}^{3\times 3} + \sin\theta_{e_1} \left[\hat{\mathbf{e}}_1 \times\right] + \left(1 - \cos\theta_{e_1}\right) \left[\hat{\mathbf{e}}_1 \times\right]^2 \tag{19}$$

$$\mathbf{E}_2 = \mathbf{I}^{3\times 3} + \sin\theta_{e_2} \left[\hat{\mathbf{e}}_2 \times\right] + \left(1 - \cos\theta_{e_2}\right) \left[\hat{\mathbf{e}}_2 \times\right]^2, \tag{20}$$

where $\mathbf{I}^{3\times 3}$ is the 3×3 identity matrix and $[\hat{\mathbf{e}}_i \times]$ is the cross-product matrix for the $i-$th error axis:

$$\left[\hat{\mathbf{e}}_i \times\right] = \begin{bmatrix} 0 & -e_{3_i} & e_{2_i} \\ e_{3_i} & 0 & -e_{1_i} \\ -e_{2_i} & e_{1_i} & 0 \end{bmatrix}. \tag{21}$$

When the two vectors are aligned the error matrix is equal to the identity matrix, as well as when they are opposite. However, this last situation is unstable for the designed ACS and, practically, the singular condition is avoided. In fact, in the case the two vectors are opposite, a small deviation from that singular condition (i.e. $\mathbf{E}_i = \mathbf{I}^{3\times 3}$ and $\theta_{e_i} = \pi\,\text{rad}$) determines a departure of the controlled system toward an error angle equal to zero. This behavior has been assessed and verified with the simulation studies conducted to design the attitude control subsystem.

The error in target angular velocity is simply defined as the vector difference between the actual angular velocity and the target one as:

$$\mathbf{e}_{\boldsymbol{\omega}} = \breve{\boldsymbol{\omega}}_T^B - \boldsymbol{\omega}_T^B, \tag{22}$$

where, being $\breve{\boldsymbol{\omega}}_T^B$ equal to $\tilde{\boldsymbol{\omega}}$, the actual angular velocity, $\breve{\boldsymbol{\omega}}_T^B$, is directly the output of the ADS.

At this point, each error measure is directly converted in a control parameter that is used to generate the required control torque. From any single error quantity, three control coefficients can be obtained, which are relative to the three orthogonal body axes, since the error quantities are evaluated in B. From the error matrices $\mathbf{E}_1$ and $\mathbf{E}_2$ two sets of control coefficients are obtained directly using the matrix elements, $\mathbf{E}_1(i,j)$ and $\mathbf{E}_2(i,j)$:

$$\mathbf{c}_1 = [\mathbf{E}_1(2,3) - \mathbf{E}_1(3,2), \mathbf{E}_1(3,1) - \mathbf{E}_1(1,3), \mathbf{E}_1(1,2) - \mathbf{E}_1(2,1)]^{\mathrm{T}} \tag{23}$$

$$\mathbf{c}_2 = [\mathbf{E}_2(2,3) - \mathbf{E}_2(3,2), \mathbf{E}_2(3,1) - \mathbf{E}_2(1,3), \mathbf{E}_2(1,2) - \mathbf{E}_2(2,1)]^{\mathrm{T}}. \tag{24}$$

Each coefficient is proportional to a component of the error axis generating the attitude error matrix (e.g. $\mathbf{E}_1(2,3) - \mathbf{E}_1(3,2)$ is proportional to the x component), in a way that the control tries to get the satellite rotating around the error axis to reduce the error angle. To better explain, if the error angles are small, the error matrices may be linearized into skew-symmetric matrices (Kane et al., 1983), whose off-diagonal components are the small rotation angles evaluated in B, which are directly represented by the control coefficients in eqs. (23) and (24). The control coefficients are passed by the control algorithm through a fourth-order Butterworth low-pass filter to smooth the control action. In this way, the control logic neglects high frequency error fluctuations that cannot be related with the real dynamics of the system and might be due to the noise produced by attitude determination subsystem. The cutoff frequency must be chosen in a way that is safely higher than a characteristic frequency of the dynamics (i.e. the orbital frequency for a Nadir pointing attitude), but also lower than the noise frequency processed by the ADS.

The control action related with the error in target directions are then simply obtained multiplying each component of the control coefficient by a dedicated gain, $k_{i_j} > 0$:

$$\mathbf{t}_1 = [k_{1_1} c_{1_1}, k_{1_2} c_{1_2}, k_{1_3} c_{1_3}]^{\mathrm{T}} \tag{25}$$

$$\mathbf{t}_2 = [k_{2_1} c_{2_1}, k_{2_2} c_{2_2}, k_{2_3} c_{2_3}]^{\mathrm{T}}, \tag{26}$$

where c_{1_i} and c_{2_i} are respectively the elements of $\mathbf{c}_1$ and $\mathbf{c}_2$. In this way, the control action is proportional to the error with respect to the target direction, producing an effect that rotates the spacecraft until the error angle is equal to zero (i.e. proportional action for the attitude control).

The control action associated with the error in angular velocity has been formulated according to the work of Avanzini et al. (2013), and it is able to drive the spacecraft toward a desired spinning condition (Note that the desired spinning condition can be also the one with all the angular rates of the satellite equal to zero). The proposed B-dot-like control law has been proven to be exponentially stable and it is particularly interesting for small satellite missions because of its simplicity and robustness to the uncertainties. Moreover, it does not require additional data with respect to those already available to be implemented. Remembering the Earth's magnetic field, which is estimated in body reference frame from the ADS as $\tilde{\mathbf{b}} = [\tilde{b}_1, \tilde{b}_2, \tilde{b}_3]^{\mathrm{T}}$, it is possible to compute it as:

$$\mathbf{t}_{\boldsymbol{\omega}} = -k_{\omega} \left(\mathbf{I}^{3\times 3} - \frac{\tilde{\mathbf{b}}\tilde{\mathbf{b}}^{\mathrm{T}}}{\left\| \tilde{\mathbf{b}} \right\|^2} \right) \mathbf{e}_{\boldsymbol{\omega}}, \tag{27}$$

where $k_{\omega} > 0$ is the gain associated with the control in angular velocity. Note that in this case no filtering action is performed to obtain $\mathbf{t}_{\boldsymbol{\omega}}$. The proposed control action is proportional to the error in angular velocity, $\mathbf{e}_{\boldsymbol{\omega}}$. However, it behaves like a derivative action for the attitude control law and, therefore, the presented fully magnetic ACS has the characteristics of a proportional derivative (PD) control system.

Finally, the overall control action, which is composed by the proportional contributions (eqs. (25) and (26)) and the derivative one (eq. (27)), is simply obtained as:

$$\mathbf{t}_c = \mathbf{t}_1 + \mathbf{t}_2 + \mathbf{t}_{\boldsymbol{\omega}}. \tag{28}$$

The output of the previous equation, if directly applied to the dynamics of the system, would ideally drive the spacecraft along the path determined by the guidance law defined in eqs. (14) to (16).

In general, the required control action $\mathbf{t}_c$ is not perpendicular to $\mathbf{b}$ and the available control torque may be different from $\mathbf{t}_c$. For this reason, the final goal of the ACS is just to compute a dipole moment able to generate a control torque, $\mathbf{t}_{mag}$, as equal as possible to the required control action. This is done exploiting again the estimated Earth's magnetic field $\tilde{\mathbf{b}}$ as:

$$\mathbf{d} = \frac{\tilde{\mathbf{b}} \times \mathbf{t}_c}{\left\| \tilde{\mathbf{b}} \right\|^2}. \tag{29}$$

The voltage to command the magnetorquers are immediately available from eq. (7) and the ACS logic is completed.

4. Subsystem Design

The attitude control subsystem design has followed a practical engineering approach, which had to be robust and easily applicable to different small satellite missions. The method has been developed directly exploiting the high-fidelity dynamical model presented in section 2, and it was intended to be ready for application on real picosatellite missions. It allows to obtain optimized performances for any mission phase, without any modification in the design process. In fact, dedicated controller gains can be computed with different optimization simulations; then, they are available on-board and they can be activated to switch between different control modes, according to mission requirements and plans.

Global optimization methods have been used to optimize the controller gains, k_{i_j} and k_ω, which guarantee the best performances for the different mission phases (e.g. de-tumbling and nominal attitude acquisition mode, maneuvering mode or nominal attitude changing mode). For example, nominal attitude acquisition mode has been optimized to have a fast attitude stabilization and to maintain the nominal pointing with good integral performances over one orbital period. It should be remembered that the system considered in this paper is subject to large disturbances and intrinsically locally under-actuated: only the variation of the geomagnetic field direction with respect to the orbital reference, if the orbit is sufficiently inclined, allows to apply orbit average torques in any direction.

The design method is based on heuristic global optimization strategies. In particular, the class of evolutionary algorithms has been selected and the genetic algorithm has proven to work well. The focus has not been directed on the particular optimization technique to be used, and no comparison between different heuristic optimization techniques has been carried out. The genetic algorithm is a method based on natural selection: an initial population composed by a random set of feasible solutions is generated and, at each optimization step, it is randomly modified keeping only the best individual solutions. The algorithm naturally evolves toward an optimal solution, following some optimization rules and satisfying the imposed constraints.

The developed method initializes the simulation with previously defined orbital and attitude initial conditions, according to the mission phases that

has to be optimized (e.g. optimization of the mission phase from random spinning attitude to initial attitude acquisition mode). All the parameters of the spacecraft, such as shape, dimensions, inertia or components data are initialized at the beginning as well. The only parameters that have to be optimized are, as already discussed, 7 controller gains: k_{1_1}, k_{1_2}, k_{1_3}, k_{2_1}, k_{2_2}, k_{2_3} and k_ω. Any set of 7 gains greater than zero forms an individual solution. In fact, the only constraint enforced on the individual solutions to create a feasible population is that all the gains must be greater than 0.

The optimization of the controller gains is formulated to achieve a long-term horizon controllability in integral sense. Thus, the fitness function, $f_m\left(k_{i_j}, k_\omega\right)$, is defined as the integral of the errors in eqs. (17), (18) and (22) over a number of n orbits:

$$f_m\left(k_{i_j}, k_\omega\right) = \int_0^{nT} \left(\delta_{e_1}\theta_{e_1} + \delta_{e_2}\theta_{e_2} + \delta_\omega \left\|\mathbf{e}_{\boldsymbol{\omega}}\right\|\right)\, dt, \tag{30}$$

where T is the orbital period, while δ_{e_1}, δ_{e_2} and δ_ω are integral weights, which are defined to nondimensionalize the integrand and to weight differently the target errors. The value of the weights is first defined according to the mission requirements, if one or two targets are more stringent than the others. Note that if any target condition is not defined, the related integrand is neglected and the optimization is performed using only one or two integrand terms. Additionally, all the integrated quantities are always positive and the absolute value is not needed.

The optimization algorithm runs a simulation for any feasible set of gains in the population and minimizes the value of $f_m\left(k_{i_j}, k_\omega\right)$ after n orbital periods. The controller gains associated to the minimum of the fitness function are a *single-run optimal solution*. To speed up the optimization process, some simulations can be interrupted in advance if certain requirements are not satisfied (e.g. pointing error is too large, de-tumbling is too slow). In this case, the cost function is heavily penalized to remove those individual solutions from the search space. To assess the robustness of a single-run solution and check its validity, the optimization is run several times with slightly different orbital and attitude initial conditions. Every time, the previously found single-run optimal solution is reinserted in the genetic algorithm and the new best solution must remain in the vicinity of the previous one. The search for the optimal set of controller gains is stopped when the difference between two successive single-run best solutions is below a certain threshold.

The feasible population is composed by 100 elements, it is initially generated with uniform distribution and, between two consecutive generations, 5 best individuals are maintained. The maximum number of allowed generations is 700 and the stopping criteria are met when there are 50 stall generations (e.g. best solution not improving for 50 iterations). On a 2.5 GHz quad core processor that runs the optimization algorithms in parallel, a single-run optimization needs less than 1 hour. The complete search and verification of the best solution may take up to 3 to 4 hours. Usually, a single mission phase tuning needs 1 or 2 days, including both computing time and operator work to set all the parameters and the validation steps.

The optimization simulations make use of the dynamical model in section 2, together with an accurate model of the major subsystems and components of a picosatellite, in order to simulate not only the spacecraft dynamics, but also the complete system. In this way, the simulations can be performed using the real data and parameters of the on-board hardware and software to practically design, test and operate the spacecraft. For example, all the magnetorquer specifications, which are available from data-sheets or experimental measurements, are inserted in the system model to have accurate values for the requested dipole and voltage, from eq. (7) and eq. (29). Then, they are exploited in the actuator model to compute the commands for the PWM voltage regulator. This step considers the saturation limits for the voltage, the quantization errors, the discrete-time signals, the delay and the noise in the command actuation. The current intensity is evaluated from the electric characteristics of the magnetorquers and this information is used to compute the generated practical magnetic dipole, $\tilde{\mathbf{d}}$, considering the non-linearity and saturation errors, the residual magnetic moment and the transient time of the electromagnetic actuators. Therefore, the real control torque inserted in the Euler's eq. (1) is $\tilde{\mathbf{t}}_{mag}$, and it is obtained from eq. (4) as:

$$\tilde{\mathbf{t}}_{mag} = \mathbf{B}(\mathbf{b})\tilde{\mathbf{d}}, \tag{31}$$

where, obviously, $\mathbf{b}$ is not the estimated geomagnetic field, but it is the real local one.

5. Reference Mission Scenario

The presented ACS has been intended for simple picosatellite missions, which are nowadays increasingly common to be launched in low Earth orbit.

These space missions are typically characterized by limited budget and not so stringent requirements that can be satisfied without excessively increasing the complexity and the cost of the spacecraft. Therefore, even if in principle the validity of the proposed control system is general, its performances aim to stabilize the spacecraft, acquire the nominal attitude within few orbits from the deployment and have a pointing accuracy in the order of 10°. Moreover, the power consumption and computing load for the on-board computer are targeted to be extremely limited, since the available resources are in the class of those typical for a picosatellite (e.g. $< 5\,\mathrm{W}$, $< 10\,\mathrm{DMIPS}$ - Dhrystone Million Instructions Per Second).

For what concern the orbital environment in which this ACS can be applied, the constraints come from the limit of the purely magnetic actuation. In fact, the inclination of the orbit must be large enough to have variation of the geomagnetic field direction in orbital reference, which is fundamental for the correct operation of such control system. Ideally, best performances are obtained in polar or nearly-polar orbits. Furthermore, the altitude is bounded from the maximum torque of the implemented magnetorquers. In fact, at low altitudes the aerodynamic torque imposes the limits for the actuator sizing, while at high altitude the weak intensity of the geomagnetic field is the limiting factor. Considering the magnetorquers that can be installed on board of a generic picosatellite, these limits correspond to a operational altitude bounded between 400 and 750 km.

The natural reference mission scenario to test the proposed ACS is therefore the one of Earth observation missions in Sun-synchronous orbit (SSO), which are typically at altitudes of $500 - 800\,\mathrm{km}$, with periods in the $90 - 100$ minute range, and inclinations of around 98°. These orbits are remarkably interesting for the class of picosatellites, allowing a nearly global coverage, a constant Sun aspect angle and a great variety of launch available for small satellites. The typical nominal attitude pointing mode in these kind of missions is the Nadir pointing one, and it is used as reference case to evaluate the performances of the control system.

Obviously, different nominal attitude modes can be simply obtained by varying target directions and target angular velocity previously defined. For example, an elementary Sun pointing can be achieved enforcing only one target direction, defined by the position of the Sun, to be aligned with one axis of the spacecraft (e.g. the solar panels normal). If the nominal attitude definition is not excessively different and the mission environment is similar no additional tuning of the controller gains is required.

The test case that is investigated in this paper considers a picosatellite with dimensions 10cm $\times$ 10cm $\times$ 3cm and mass of 350 g. The attitude determination subsystem is composed by an IMU, a magnetometer and a Sun sensor capable to estimate the attitude within ~ 0.5 deg of accuracy on each axis and ~ 0.01 rad/s of precision on the angular rates. The 3 PCB-embedded magnetorquers are 9cm $\times$ 9cm or 9cm $\times$ 2.5cm coils, composed by 6 layers of 25 turns each. The larger one is mounted on the 10cm $\times$ 10cm face and is able to produce at maximum 1.5×10^{-3} mNm of torque in polar region and 7.5×10^{-4} mNm at the equator. The smaller ones are installed on the 10cm $\times$ 3cm faces and their maximum torque at the poles is 5×10^{-4} mNm, while at the equator is 2.5×10^{-4} mNm. The expected disturbances in a 600 km SSO for a picosatellite of the size considered in this work, generate torques below 2.5×10^{-5} mNm. Hence, the assumed magnetorquers are fully sufficient to control the small spacecraft. The disturbances are computed assuming coefficient of solar radiation absorption $c_a = 0.8$ and reflection $c_r = 0.2$; drag coefficient $C_d = 2.2$ and internal residual dipole in the order of 5×10^{-4} Am^2. However, this last parameter will be discussed with more detail in the next section.

The nominal attitude can be defined, with reference to fig. 3, as the one with one small face ($\hat{\mathbf{b}}_3$) pointed to Earth and a large face ($\hat{\mathbf{b}}_1$) aligned with the horizontal direction, in order to be almost aligned with the velocity vector reducing the natural decay time. The spinning axis to maintain the Nadir pointing must be parallel to the normal to the remaining small face ($\hat{\mathbf{b}}_2$) and the spinning rate must be defined to perform one rotation per orbit: the angular rate of the spacecraft should be equal to the orbital angular rate with spinning axis aligned with the LVLH third axis, $\hat{\mathbf{z}}_L$. Therefore, the first target direction is the LVLH vertical axis, $\hat{\mathbf{x}}_L$, while the second direction is defined as the LVLH horizontal axis, $\hat{\mathbf{y}}_L$.

The actual target directions are therefore evaluated, from eqs. (11) and (12), as:

$$\breve{\mathbf{v}}_{T_1}^B = \tilde{\mathbf{P}}\hat{\mathbf{x}}_L \tag{32}$$

$$\breve{\mathbf{v}}_{T_2}^B = \tilde{\mathbf{P}}\hat{\mathbf{y}}_L. \tag{33}$$

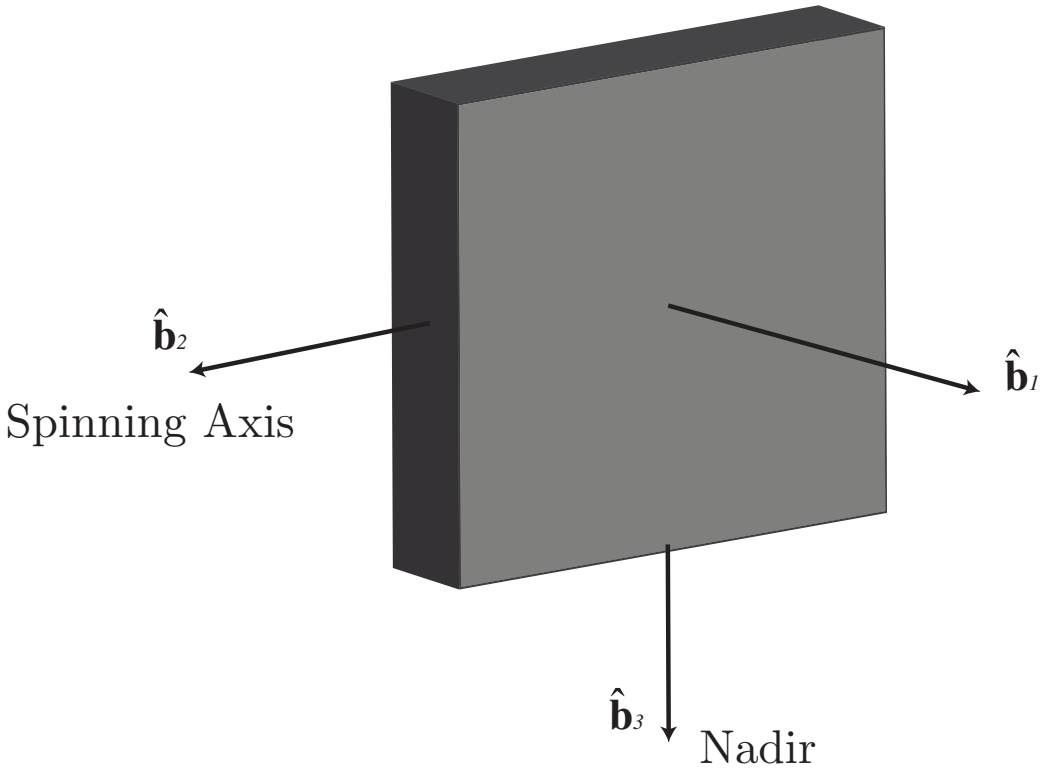

Figure 3: Body-fixed frame and nominal attitude.

Moreover, the target definitions in eqs. (8) to (10) become:

$$\mathbf{v}_{T_1}^B = -\hat{\mathbf{b}}_3 \tag{34}$$

$$\mathbf{v}_{T_2}^B = -\hat{\mathbf{b}}_1 \tag{35}$$

$$\boldsymbol{\omega}_T^B = \dot{\theta}\,\hat{\mathbf{b}}_2, \tag{36}$$

where $\dot{\theta}$ is the orbital angular velocity, which is constant only for a circular orbit. Thus, eq. (36) is variable in time for elliptic orbits and the ADS has to determine the orbital rate according to the orbital position.

The reference mission scenario has been used to tune the attitude control subsystem once. All the simulations that will be discussed next have been obtained with an optimal set of controller gains, which have been computed and validated with 12 runs of the optimization algorithm.

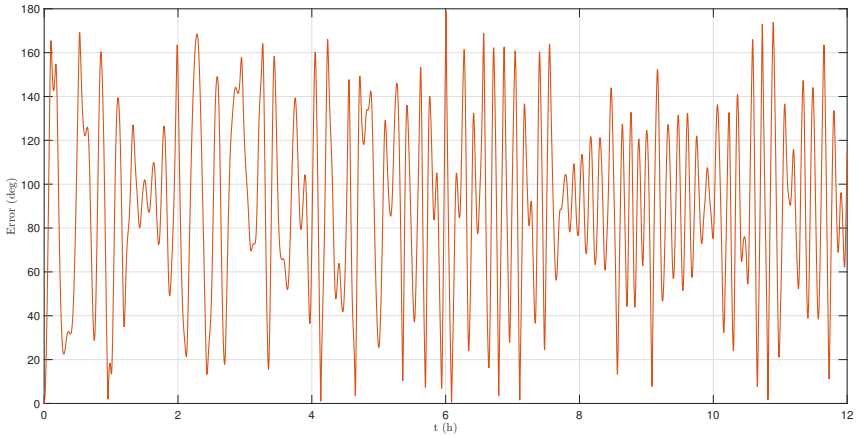

Figure 4: Nadir error angle, θ_{e_N}, in uncontrolled attitude dynamics.

6. Simulation Results

The simulations presented here refer to the test reference mission scenario described in the previous section. This paper focalizes its attention on this single mission scenario because it has been extensively tested and verified, together with the ADS logic, for the implementation of a real picosatellite mission to be launched in-orbit. Details on the practical and hardware implementation of the ACS currently discussed, which is still on-going and not yet completed at time of writing, will be presented in a dedicated publication. Nevertheless, the presented attitude control subsystem logic and design technique have been preliminarily assessed also on different mission environments, with different targets and spacecraft characteristics. In all the situations, the obtained results agree with those that are discussed in this section, leading to analogous overall conclusions and remarks with general validity and relevance.

The natural dynamics to be controlled by the developed attitude control subsystem is in general extremely chaotic and strongly dependent from the interaction between the internal residual dipole and the geomagnetic field. This is evident from the uncontrolled attitude dynamics reported in fig. 4, where it is shown the error angle, θ_{e_N}, computed with respect to the Nadir target direction. In this simulation, the spacecraft is initially single spin and its axes are aligned as described in section 5 (i.e. errors equal to 0 at $t = 0$). These conditions should lead to a gravity gradient stabilized attitude dynamics. However, this is not the case for a picosatellite, whose inertia properties are

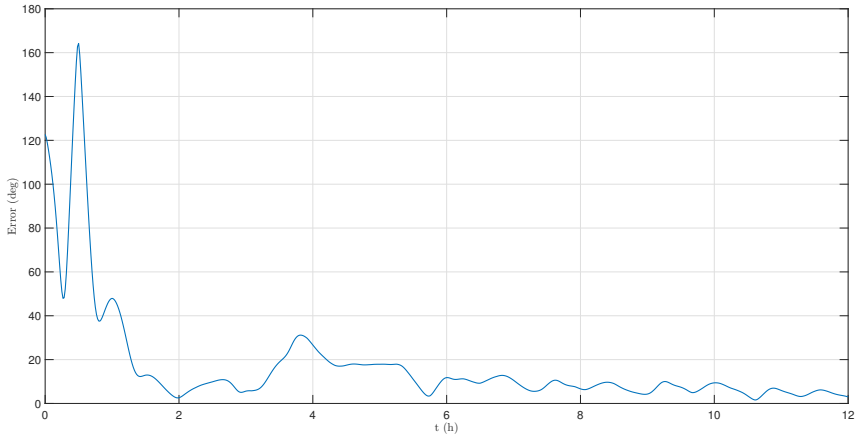

Figure 5: Nadir error angle, θ_{e_N}, in controlled attitude dynamics.

low compared to the magnetic density due to the on-board electronics, and the resulting dynamics is an erratic motion useless for picosatellite applications.

The performances of the designed and tuned ACS are evident in fig. 5. They are achieved by using an optimal set of gains, result of the design method described in section 4, and they are applied to the reference mission scenario previously defined. The simulation is initialized with random attitude dynamics at $t = 0$. In particular, the spacecraft has an initial Nadir error angle of $\sim 120\,\text{deg}$ and is tumbling. The ACS is able to de-tumble the spacecraft in ~ 1 orbital period and correctly align the Nadir face with an error angle, θ_{e_N}, in the order of 10 deg. The figure shows only the error angle and not the error axis, because this is the sizing quantity to be assessed to check the performances of the control system. The evolution of the error axis is strongly dependent from the initial error axis and it is almost constant when the associated error angle is large enough (i.e. control system rotates the spacecraft around a single axis to reduce the large proportional error in a small time). Obviously, the error axis starts to have a chaotic evolution when the error angle is small and the controller command torques in any direction to stabilize the motion about the nominal condition. The dynamics shown in figs. 4 and 5 has been simulated in a 600 km circular SSO (Local Time of the Ascending Node - $LTAN = 12.00$) for ~ 8 orbital periods. In these simulations, the internal residual dipole of the spacecraft has been assumed

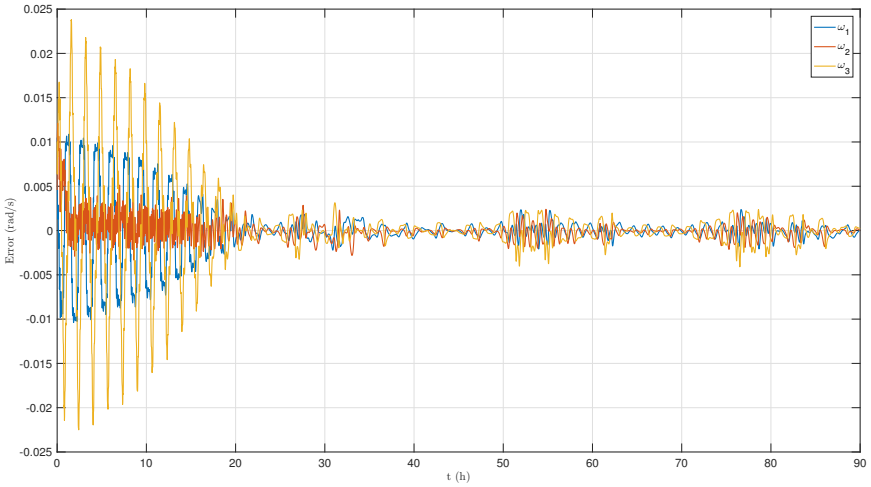

Figure 6: Error angular velocity, $\mathbf{e}_{\boldsymbol{\omega}}$, during de-tumbling in controlled attitude dynamics.

constant in time, in a random direction mainly aligned with $\hat{\mathbf{b}}_1$ (fig. 3) and with magnitude $5 \times 10^{-4}\,\mathrm{Am}^2$.

The de-tumbling phase is more evident in fig. 6, where the spacecraft is started in an extremely chaotic tumbling motion, compatible with the worst-case release specifications from typical picosatellite orbital deployer (P-POD). The simulation environment is again a 600 km circular SSO with $LTAN = 12.00$ and the simulation time is $\sim$ 60 orbital periods. The de-tumbling of the spacecraft and the acquisition of the desired spinning condition is completed in less than 1 day ($\sim$ 15 orbital periods), then the desired motion is maintained within $\sim 0.005\,\mathrm{rad/s}$ in any body axis. The ripples in the angular velocity error are due to the fact that, in this case, the controller is continuously trying to enforce three different target conditions. Moreover, the higher error periods at $t \simeq 50\,\mathrm{h}$ and $t \simeq 75\,\mathrm{h}$ are a particular feature of this type of attitude control subsystem.

This feature can be analyzed and discussed looking at fig. 7, where the orbital dynamics and all the spacecraft parameters are initialized as in the previous cases. The rotational motion has random initial attitude and spinning conditions, simulating again the release from the P-POD. The three plots report all the three errors from the target conditions in eqs. (34) to (36), and the simulation runs for $\sim 4\,\mathrm{d}$. In this case, the attitude control subsystem de-tumbles the spacecraft in about 5 h and acquires nominal pointing

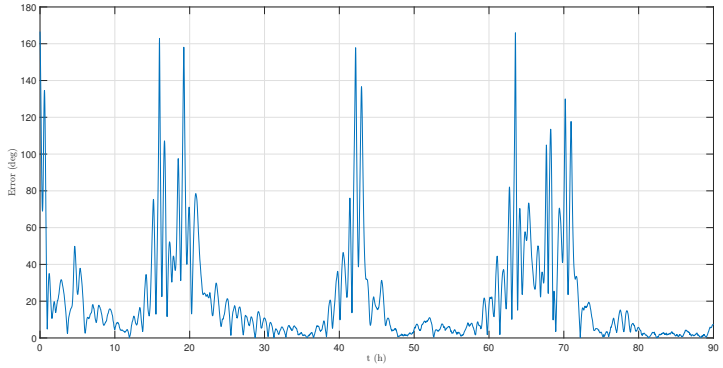

(a) Nadir error angle, θ_{e_N}.

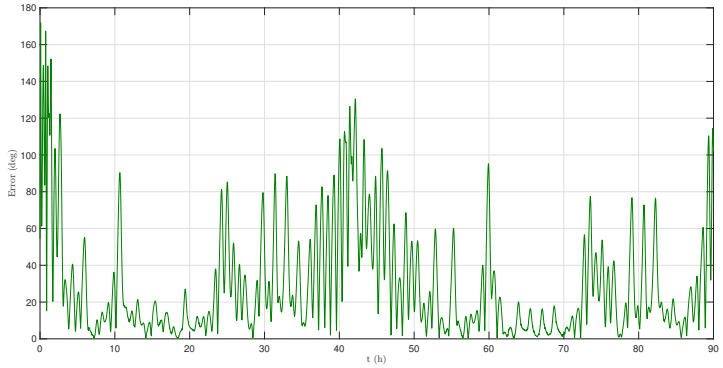

(b) Horizontal error angle, θ_{e_H}.

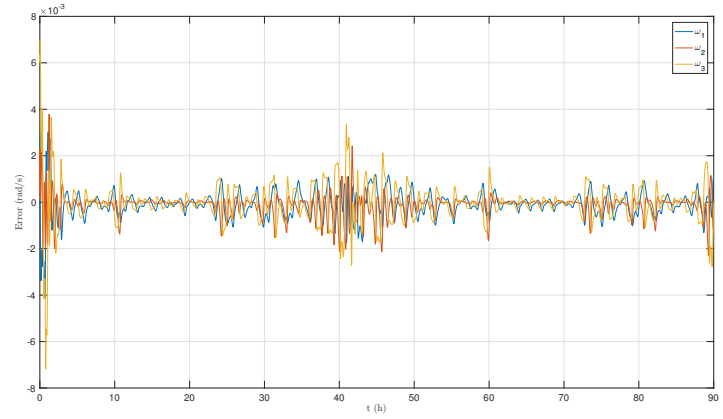

(c) Error angular velocity, $\mathbf{e}_{\boldsymbol{\omega}}$.

Figure 7: Controlled attitude dynamics.

approximately in 10 h. The attitude tuning has been performed considering a higher priority for the Nadir target direction with respect to the horizontal target, as can be realized comparing fig. 7a with respect to fig. 7b.

The nominal nadir pointing is lost 3 times in this simulation, and the loss of precision repeats every 24 h. This behavior is unavoidable and characterizes the designed ACS with this peculiar feature, which can be explained considering the physics of the problem. In fact, the picosatellite is controlled in average along one orbit by an under-actuated control system which in some cases may be not effective to counteract the system departure from the desired state. Moreover, an increase in disturbance sensitivity at high frequency is present and the closed-loop system interaction with the Earth's magnetic field is affected by the higher order harmonics of the geomagnetic field.

For example, with reference to the case presented in fig. 7, the loss in control authority happens above an Earth's region where the magnetic field in body reference, $\mathbf{b}$, has a larger component b_2 while in nominal attitude. Since the required control torque is mainly around $\hat{\mathbf{b}}_2$, looking at the explicit expression of the magnetorquer control action in eq. (4):

$$\mathbf{t}_{mag} = [b_3 d_2 - b_2 d_3, b_1 d_3 - b_3 d_1, b_2 d_1 - b_1 d_2]^{\mathrm{T}}, \tag{37}$$

the generated dipole has component primarily along $\hat{\mathbf{b}}_1$, d_1, and along $\hat{\mathbf{b}}_3$, d_3. Hence, the generated dipole and the local direction of $\mathbf{b}$ determine large spurious torques around the body axes 1 and 3, which leads to the departure from the nominal pointing mode. From this fact, the limitations of a purely magnetic ACS are evident: when the requested control torque is aligned with the Earth's magnetic field, the system cannot be completely controlled. In addition to this, the higher harmonics of b determines a resonance condition that explodes when the system is not controllable. In fact, the same simulation with a dipole model of the geomagnetic field results in similar loss of pointing periods, but the peaks are lower than those in fig. 7a. Both the critical magnetic field orientation, associated with the under-actuation of magnetic control, and the small variations of the magnetic disturbances, associated with the increase in disturbance sensitivity, contributes to the resulting dynamics of the system.

The overall behavior is dependent from the close-loop dynamics that has been tuned minimizing the error on simulations time span $t > 24$ h, in order to catch the periodicity in the disturbances and reduce resonances. Thus, the

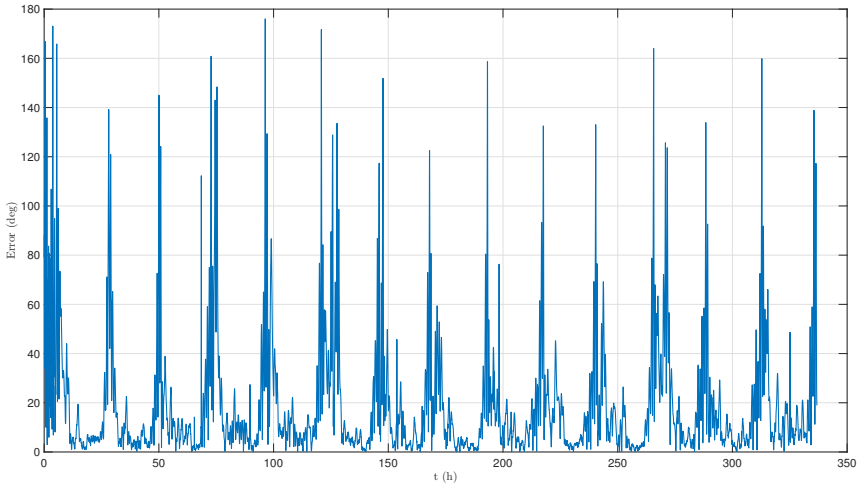

Figure 8: Nadir error angle, θ_{e_N}, in controlled attitude dynamics for a simulation time equal to the nominal picosatellite's lifetime, $t \simeq 14d$.

system is stable in average over the period of the disturbances, and the loss of pointing is necessary to control the system for large time periods. In fact, the ACS is always able to recover from the n of control authority and come back to nominal operation guaranteeing a period of good pointing accuracy, within the requirements of typical picosatellite missions (10 deg-15 deg).

These performances have been assessed also with long time simulations, like the one reported in fig. 8. In this case, the nominal lifetime of the picosatellite ($\sim 14d$) has been simulated and the behavior of the system is always the same: a loss of pointing every ~ 24 h when the spacecraft is over a certain region of the Earth. The precise region depends from orbit inclination, LTAN and nominal attitude pointing. For the spacecraft presented in this paper, the region associated with the begin of the loss of pointing period is the one above eastern Russia, Korea and Japan. Obviously, the spacecraft is correctly pointed for several orbits before the next misalignment phase occurs. The closed-loop cycle dynamics is basically a series of continuous de-tumbling and nominal attitude acquisition phases.

The validation campaign has been conducted over SSO with different altitudes, eccentricities and LTAN. The system has proven to be robust also to different attitude injection conditions: the ACS is able to de-tumble the spacecraft within few orbital periods from any initial attitude and spinning

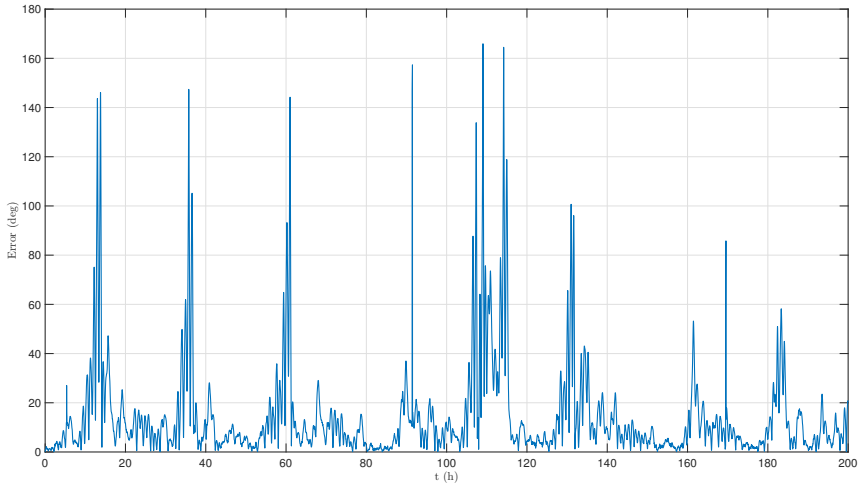

Figure 9: Nadir error angle, θ_{e_N}, in controlled attitude dynamics starting from nominal attitude initial conditions.

condition (e.g. de-tumble time between 2 h and 15 h). Also the ideal case of correct injection of the spacecraft in nominal attitude dynamics, reported in fig. 9, shows the peculiar behavior of the presented ACS. Different orbit inclination, eccentricity and LTAN do not affect the overall performances of the ACS. Only the position of the area associated with the begin of the loss of pointing period is affected by these orbital parameters. The altitude of the orbit is another factor that is not relevant for system's controllability, as long as the altitude boundaries are within the tolerances imposed by typical error injection performances of common launchers. In fact, no significant loss of ACS precision is observed if the altitude is in the order of ± 200 km from the nominal one. Nevertheless, the results of the simulation campaign showed that the orbit's perigee must be above ~ 300 km. Below such threshold, drag torque cannot be compensated with the designed control law and the nominal magnetorquers; thus, the dynamics is completely chaotic and influenced by the strong aerodynamic torques.

Another important aspect to be assessed is the dependence of the designed ACS from the internal residual dipole of the spacecraft. This parameter is indeed very difficult to estimate and is greatly influenced from the internal electronics. Thus, a sensitivity analysis is very useful to validate the results of the algorithms. As already mentioned, the internal residual dipole of a

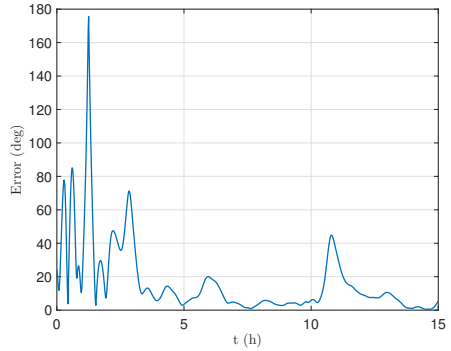

(a) Constant $\mathbf{d}_{res}$, mainly aligned with principal axis $\hat{\mathbf{b}}_1$.

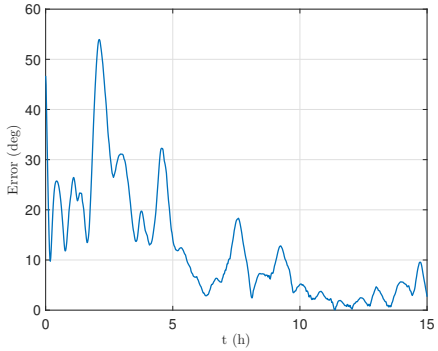

(b) Constant $\mathbf{d}_{res}$, aligned with a casual direction.

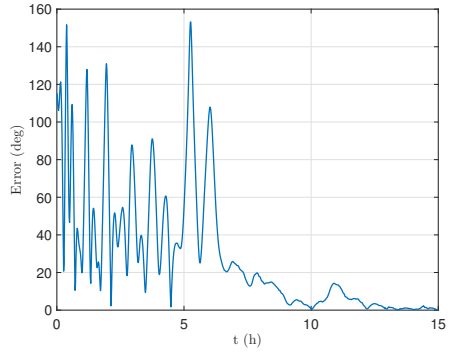

(c) Variable $\mathbf{d}_{res}$, mainly aligned with principal axis $\hat{\mathbf{b}}_1$.

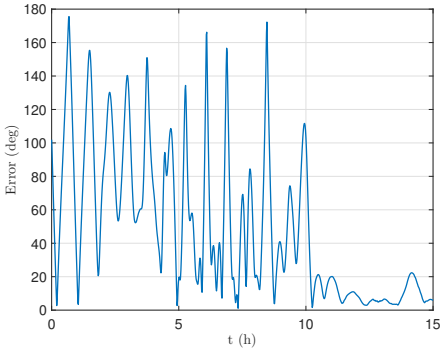

(d) Variable $\mathbf{d}_{res}$, aligned with a casual direction.

Figure 10: Internal residual dipole comparison: $\|\mathbf{d}_{res}\| = 5 \times 10^{-4}\,\mathrm{Am}^2$.

picosatellite, $\mathbf{d}_{res}$, is in the order of $5 \times 10^{-4}\,\mathrm{Am}^2$ and it is typically mainly aligned with the normal to face containing the most electric loops (e.g. the face where the electronic boards are mounted). The sensitivity analysis has been carried out with respect to the dipole magnitude, direction and variability. The first parameter has proven to be not so relevant within the values that are reasonable for such a small spacecraft. In fact, as long as the magnetorquers are correctly sized, the different magnitudes of $\mathbf{d}_{res}$ are completely manageable. Instead, the sensitivity to the other parameters is more interesting to be tested. In fig. 10, representative simulations for different typologies of internal residual dipoles are shown. For the considered case in fig. 3, the dipole is probably aligned with $\hat{\mathbf{b}}_1$, since the electronic

boards are mounted normally to that principal axis. Therefore, cases in which the dipole is mainly aligned with that direction (fig. 10a and fig. 10c) are compared to situations where the dipole is in a completely random direction (fig. 10b and fig. 10d). Moreover, a dipole that is constant in time (fig. 10a and fig. 10b) is compared also with one that is time variable (fig. 10c and fig. 10d). Just for clarification, the dipole that is variable in time and it is also mainly aligned with $\hat{\mathbf{b}}_1$ can be represented as a dipole that varies within a cone aligned with the first principal direction of the spacecraft.

The results of the simulations reported in these pictures can be used to draw general consideration on the different typologies of $\mathbf{d}_{res}$. In fact, the dipole aligned in a random direction determines worse performances of the ACS, since this has been sized considering the dipole mainly aligned with $\hat{\mathbf{b}}_1$. Hence, the developed method must be tuned on the engineering model of the spacecraft to have a ready to fly ACS in a fast and very practical way. Moreover, the variable dipole cases are more difficult to be managed, but the performances are anyway within the imposed design requirements. In general, the proposed ACS has proven to be robust to any class of internal residual dipole, being able to de-tumble and control a picosatellite in any situation.

7. Final Remarks

This paper was intended to present the control logic and the design method to develop a fully magnetic attitude control subsystem for picosatellites. Many simulations, for different mission scenarios and different nominal attitude dynamics, have been carried out to test and verify the obtained control algorithms. The performances are always compatible with those presented in this paper, which have been obtained by using the optimal gains for the selected reference mission.

The necessity of an active attitude control subsystem is resulted to be real to achieve sufficient stabilization and pointing performances with a picosatellite. Passive gravity gradient or spinning stabilization techniques proven to be not sufficient for such small low inertia satellites. Fully magnetic actuation has been selected for simplicity and reliability. Furthermore, thrusters and reaction wheels could not be used due to size and mass constraints.

The proposed control logic is robust enough and it can be implemented on-board within memory and processor constraints. The design method follows a practical engineering approach that is easily scalable to any kind of small satellite mission. Moreover, the tuning of the control subsystem is

directly performed on the high-fidelity dynamical and systems models through a heuristic global optimization method. In this way, the controller parameters can immediately be implemented for testing and integration on real hardware.

The fully magnetic attitude control subsystem has been developed together with a dedicated efficient and effective attitude determination subsystem for picosat. At time of writing, the whole attitude determination and control logic is currently being implemented on the real hardware. Future works will conduct an extensive hardware-in-the-loop verification of the control logic and the system actuation will be tested on ground.

From the analyses carried out with simulated system and dynamics, the fully magnetic ACS satisfies the imposed constraints and achieves the goals for typical picosatellite missions. Pointing accuracy is low, but within the constraints of typical picosatellites payloads (10 deg-15 deg). Closed loop dynamics is stable and, even if a loss of pointing is expected and periodic, the ACS is always able to fully recover the nominal attitude. For a single optimal set of the controller gains, the system proved to be robust to uncertainties in orbital parameters, system deployment and injection, spacecraft characteristics and internal residual dipole typologies.

Finally, it is significant to mention that, in terms of power consumption, the proposed ACS is very suitable for picosatellites, as the magnetorquers absorb at maximum 1×10^{-3} W - 1×10^{-2} W of electric power, while typical picosatellites can produce in average 5×10^{-1} W - 2.5 W of power from body mounted solar panels.

Acknowledgments

The authors would like to acknowledge the support of GP Advanced Projects Srls in the development of the presented ACS for picosat platforms and the opportunity offered to test this control algorithms in-orbit, during the operations of the picosatellite FEES (Colagrossi et al., 2016, 2017).

References

Avanzini, G., De Angelis, E. L., and Giulietti, F. (2013). Acquisition of a desired pure-spin condition for a magnetically actuated spacecraft. *Journal of Guidance, Control, and Dynamics*, 36(6):1816–1821.

Avanzini, G. and Giulietti, F. (2012). Magnetic detumbling of a rigid spacecraft. *Journal of Guidance, Control, and Dynamics*, 35(4):1326–1334.

Bate, R. R., Mueller, D. D., and White, J. E. (1971). *Fundamentals of astrodynamics*. Dover Publications Inc., New York.

Bhat, S. P. and Dham, A. S. (2003). Controllability of spacecraft attitude under magnetic actuation. In *42nd IEEE Conference on Decision and Control, 2003*, volume 3, pages 2383–2388.

Colagrossi, A., Bucci, L., Lavagna, M., and Parissenti, G. (2016). GNC design and testing for an IOD/IOV 1/3U platform. Presentation presented at the 8th European CubeSat Symposium: Nanosatellites for Science and Technology, September 2016, London, UK.

Colagrossi, A., Bucci, L., Lavagna, M., and Parissenti, G. (2017). Three-axis active and fully magnetic attitude control design for a 1/3U picosat platform. Paper presented at the 8th Nano-Satellite Symposium, June 2017, Matsuyama, JP.

Cubas, J., Farrahi, A., and Pindado, S. (2015). Magnetic attitude control for satellites in polar or sun-synchronous orbits. *Journal of Guidance, Control, and Dynamics*, 38(10):1947–1958.

Flatley, T., Morgenstern, W., Reth, A., and Bauer, F. (1997). A B-dot acquisition controller for the RADARSAT spacecraft. In *Flight mechanics symposium: NASA Conference Publication*, volume 3345, pages 79–90.

Inamori, T., Sako, N., and Nakasuka, S. (2011). Magnetic dipole moment estimation and compensation for an accurate attitude control in nano-satellite missions. *Acta Astronautica*, 68(11):2038–2046.

Kane, T. R., Likins, P. W., and Levinson, D. A. (1983). *Spacecraft dynamics*. McGraw-Hill Book Co., New York.

Lovera, M. and Astolfi, A. (2004). Spacecraft attitude control using magnetic actuators. *Automatica*, 40(8):1405–1414.

Lovera, M., De Marchi, E., and Bittanti, S. (2002). Periodic attitude control techniques for small satellites with magnetic actuators. *IEEE Transactions on Control Systems Technology*, 10(1):90–95.

Markley, F. L. and Crassidis, J. L. (2014). *Fundamentals of spacecraft attitude determination and control*. Space Technology Library, Springer, New York.

Musser, K. L. and Ebert, W. L. (1989). Autonomous spacecraft attitude control using magnetic torquing only. In *Flight mechanics / Estimation theory symposium: NASA Conference Publication*, volume 3050, pages 23–38.

Schalkowsky, S. and Harris, M. (1969). Spacecraft magnetic torques. Technical Report NASA/SP-8018, NASA Space Vehicle Design Criteria.

Sidi, M. J. (1997). *Spacecraft dynamics and control: a practical engineering approach*. Cambridge University Press, Cambridge.

Silani, E. and Lovera, M. (2005). Magnetic spacecraft attitude control: a survey and some new results. *Control Engineering Practice*, 13(3):357–371.

Stickler, A. C. (1972). A magnetic control system for attitude acquisition. Technical Report NASA-CR-130145, REPT-90345, Ithaco, Inc.

Stickler, A. C. and Alfriend, K. (1976). Elementary magnetic attitude control system. *Journal of spacecraft and rockets*, 13(5):282–287.

Wertz, J. R. (1978). *Spacecraft Attitude Determination and Control*. D. Reidel Publishing Co., Dordrecht.

White, J. S., Shigemoto, F. H., and Bourquin, K. (1961). Satellite attitude control utilizing the earth's magnetic field. Technical Report NASA-TN-D-1068, A-474, NASA Spacecraft Design, Testing and Performance.

Wiśniewski, R. and Blanke, M. (1999). Fully magnetic attitude control for spacecraft subject to gravity gradient. *Automatica*, 35(7):1201–1214.